NANO LETTERS

2008
Vol. 8, No. 7
2012-2016

Substrate-Free Gas-Phase Synthesis of Graphene Sheets

Albert Dato,*,† Velimir Radmilovic,‡ Zonghoon Lee,‡ Jonathan Phillips,§ and Michael Frenklach||

Applied Science and Technology Graduate Group, University of California, Berkeley, California 94720, National Center for Electron Microscopy, Lawrence Berkeley National Laboratory, Berkeley, California 94720, Los Alamos National Laboratory, Los Alamos, New Mexico 87545, and Department of Mechanical Engineering, University of California, Berkeley, California 94720

Received April 23, 2008; Revised Manuscript Received May 22, 2008

ABSTRACT

We present a novel method for synthesizing graphene sheets in the gas phase using a substrate-free, atmospheric-pressure microwave plasma reactor. Graphene sheets were synthesized by passing liquid ethanol droplets into an argon plasma. The graphene sheets were characterized by transmission electron microscopy, electron energy loss spectroscopy, Raman spectroscopy, and electron diffraction. We prove that graphene can be created without three-dimensional materials or substrates and demonstrate a possible avenue to the large-scale synthesis of graphene.

Graphene, an atomically thin sheet of carbon atoms tightly packed in a two-dimensional (2D) honeycomb lattice, possesses many extraordinary properties, and its potential applications have recently been the subject of intense scientific interest.[1–11] However, obtaining graphene sheets is a challenge. Methods developed thus far rely on three-dimensional (3D) crystals[1–9] or substrates[10–14] to obtain 2D graphene. These techniques include the micromechanical cleavage of graphite,[1–6] the chemical reduction of exfoliated graphite oxide,[7–9] the vacuum graphitization of silicon carbide substrates,[10,11] and the growth of graphene on metal substrates.[12–14]

Many of the current plasma techniques aimed at synthesizing carbon nanostructures have involved plasma enhanced chemical vapor deposition (PECVD). These methods have required substrates and low-pressure environments (below 10 Torr) to obtain carbon nanostructures. The synthesis and growth of these materials proceeded via surface reactions and hence were dependent on substrate conditions. For example, radio frequency PECVD[15–17] has been used to create "carbon nanosheets" on various temperature- and bias-controlled substrates, while dc PECVD[18] and microwave PECVD[19,20] have been used to form "carbon nanowalls" on quartz substrates and metallic growth stages, respectively. Nanostructures were grown in time scales on the order of minutes to hours, and graphene sheets obtained by these methods were formed either on the substrate,[15–20] bulk layers of graphite,[15] or 3D carbon structures.[19,20] We have synthesized graphene sheets using a substrate-free method that is fundamentally different from PECVD. Graphene sheets were created directly in the gas phase, and the entire synthesis process took place in fractions of a second, in an atmospheric-pressure environment.

Substrate-free microwave plasma reactors have been used in the past to synthesize various materials. Carbon nanostructures, such as nanodiamond, have been synthesized in the gas phase in low-pressure (below 150 Torr) microwave plasma reactors.[21] Advances in microwave plasma reactor technology resulted in the development of reactors capable of operating at atmospheric pressures. These reactors have been used to obtain aluminum nanoparticles[22] and spherical boron nitride particles.[23]

Present experiments were carried out in an atmospheric-pressure microwave (2.45 GHz) plasma reactor (Figure 1a). A quartz tube (21 mm internal diameter) located within the reactor was used to pass an argon gas stream (1.71 L/min) through a microwave guide. This stream was used to generate an argon plasma. A smaller alumina tube (3 mm internal diameter) located concentrically within the quartz tube was used to send an aerosol consisting of argon gas (2 L/min) and ethanol droplets (4×10^{-4} L/min) directly into the argon plasma. Ethanol droplets had a residence time on the order of 10^{-1} s inside the plasma. During this very brief period of

* Corresponding author, amdato@me.berkeley.edu.
† Applied Science and Technology Graduate Group, University of California.
‡ National Center for Electron Microscopy.
§ Los Alamos National Laboratory.
|| Department of Mechanical Engineering, University of California.

10.1021/nl8011566 CCC: $40.75
Published on Web 06/05/2008

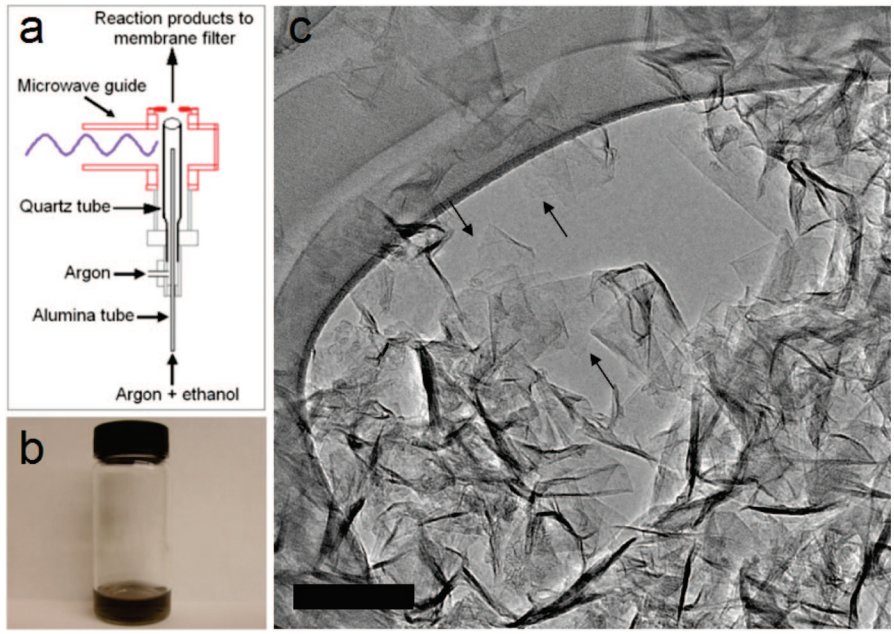

Figure 1. Synthesis of graphene sheets. (a) Schematic of the atmospheric-pressure microwave plasma reactor used to synthesize graphene. (b) Photograph of graphene sheets dispersed in methanol. (c) A typical TEM image of graphene sheets freely suspended on a lacey carbon TEM grid. Homogeneous and featureless regions (indicated by arrows) indicate regions of monolayer graphene. Scale bar represents100 nm.

time, ethanol droplets rapidly evaporated and dissociated in the plasma, forming solid matter. After passing through the plasma, reaction products underwent rapid cooling and were collected downstream on nylon membrane filters. The rate of solid carbon material collected on the filters was 2 mg/min, for a mass input of carbon in the ethanol of 164 mg/min.

Graphene sheets collected on the filters were sonicated in methanol for 5 min. The sheets were found to easily disperse during sonication, resulting in the formation of a homogeneous black suspension (Figure 1b). Droplets of the suspension were deposited on lacey carbon grids for electron microscopy analysis. A 200 kV Philips CM200/FEG transmission electron microscope equipped with a Gatan Imaging Filter was used to characterize the graphene sheets by transmission electron microscopy (TEM) and electron energy loss spectroscopy (EELS). The graphene sheets were found to be stable under ambient conditions. Some graphene sheets were characterized over 6 months after synthesis.

Single-layer and bilayer graphene sheets were synthesized at 250 W of applied microwave power. The sheets were freely suspended on a lacey carbon TEM grid and appeared as continuous, crumpled sheets exhibiting homogeneous and featureless regions (Figure 1c). Previous TEM studies of graphene[5,6] utilized a combination of TEM imaging and nanobeam electron diffraction patterns to prove that regions of graphene sheets that appeared homogeneous and featureless were regions of monolayer graphene. Less transparent areas can be attributed to the folding and overlap of a single sheet or the overlap of multiple sheets, and the darkest areas are a result of crumpled regions. It can be observed that the sheets are folded in some locations, and it is possible to determine the number of graphene layers in a sheet because of the clear TEM signature provided by these regions.[5,6] Folded regions are locally parallel to an electron beam, and single-layer graphene has been found to exhibit one dark line, similar to TEM images of single-walled carbon nanotubes.[5] Bilayer and few-layer graphene sheets have been found to exhibit multiple dark lines in folded regions, such as in the case of multiwalled nanotubes.[5] The monolayer graphene sheets synthesized in our experiments exhibited a single dark line (Figure 2a), while bilayer graphene sheets had two dark lines (Figure 2b). Interlayer distances were determined by measuring the spacing of the dark fringes. Using GATAN Digital Micrograph 3 software, the average interlayer spacing in the bilayer sheet was determined to be 0.335 nm with a standard deviation of $\pm$0.005 nm.

After TEM images were obtained, EELS spectra in the carbon K-edge region were used to investigate the structure of the synthesized sheets. EELS has been used to unambiguously distinguish between different carbon films, such as diamond, graphite, and amorphous carbon.[24–26] The main features of a graphite EELS spectrum in the carbon K-edge region are a peak at 285 eV that corresponds to transitions from the 1s to the π^* states ($1s-\pi^*$), and a peak at 291 eV that corresponds to transitions from the 1s to the σ^* states ($1s-\sigma^*$).[24–26] The graphitic structure of the monolayer sheet shown in Figure 2a was confirmed by its corresponding EELS spectrum (Figure 2c), which exhibited the $1s-\pi^*$ and $1s-\sigma^*$ peaks at 285 and 291 eV, respectively. The EELS spectrum for the bilayer graphene sheet (Figure 2d) also exhibited these characteristics.

EELS was also used to investigate the presence of oxygen, hydrogen, and OH on the graphene sheets. Hydrogen and oxygen K-edge peaks occur at 13 and 532 eV, respectively, while OH peaks have been reported to occur at 528 eV.[27,28]

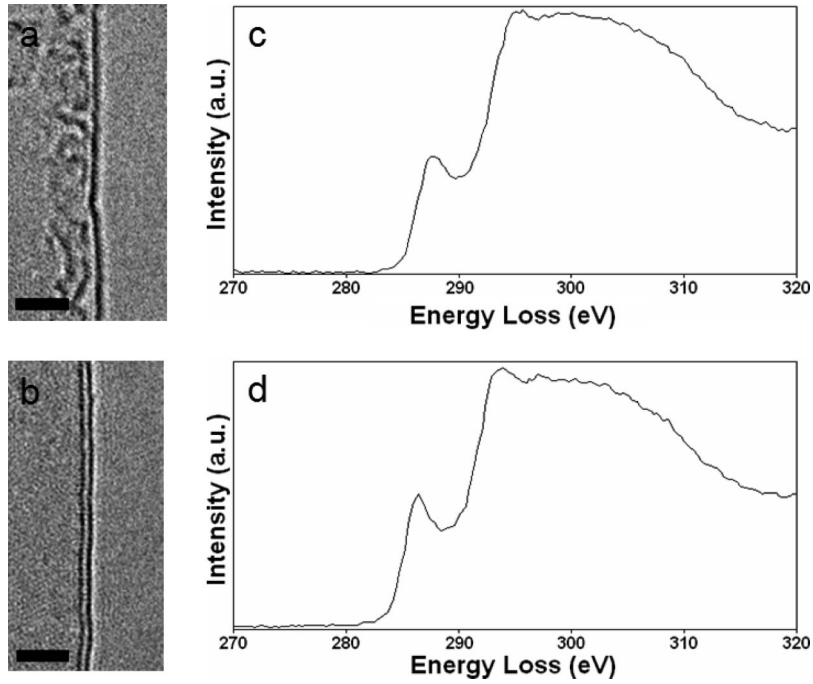

Figure 2. TEM and EELS characterization. TEM images of (a) single-layer and (b) bilayer graphene. Scale bars represent 2 nm. Corresponding EELS spectra taken from the (c) single-layer sheet and (d) bilayer sheet. These spectra exhibit the characteristics of bulk graphite.

The sheets exhibited no detectable hydrogen, oxygen, and OH EELS spectra, which indicated that the sheets were pure carbon.

Raman spectroscopy characterization was also performed. Synthesized materials were placed on a silicon substrate, and Raman spectra from a region on the substrate were obtained using a SPEX 1877 0.6 m triple spectrometer at 488 nm, with a 5 cm^{-1} spectral resolution. Measurements were performed with an incident power of 40 mW using a spot size of 300 μm $\times$ 120 μm. The most prominent feature in the Raman spectrum of graphene is the 2D peak, and its position and shape can be used to clearly distinguish between single-layer, bilayer, and few-layer graphene.[6,29] Single-layer graphene sheets have a single, sharp 2D peak[6,29,30] below 2700 cm^{-1}, while bilayer sheets have a broader and upshifted 2D peak[6,29] located at $\sim$2700 cm^{-1}. Sheets with more than five layers and bulk graphite exhibit similar spectra,[6,29] which have broad 2D peaks that are upshifted to positions greater than 2700 cm^{-1}. The Raman spectrum obtained from the synthesized sheets exhibited a single, sharp 2D peak at $\sim$2670 cm^{-1} (Figure 3a), indicating that the analyzed region consisted of single-layer graphene.

The position and shape of the G peak shown in Figure 3b provided further evidence that graphene was synthesized. The G peak for graphene sheets[29,30] occurs at $\sim$1580 cm^{-1}, and this peak broadens and significantly shifts to 1594 cm^{-1} for graphite oxide sheets.[8,9] The G peak of the synthesized sheets is located at $\sim$1580 cm^{-1}, which shows that oxygen from the ethanol precursor was not present on the graphene sheets.

The appearance of a D peak at $\sim$1350 cm^{-1} and a D′ shoulder at $\sim$1620 cm^{-1} has been attributed to the presence of structural disorder in graphene sheets.[29] Although these features were present in the Raman spectrum of the

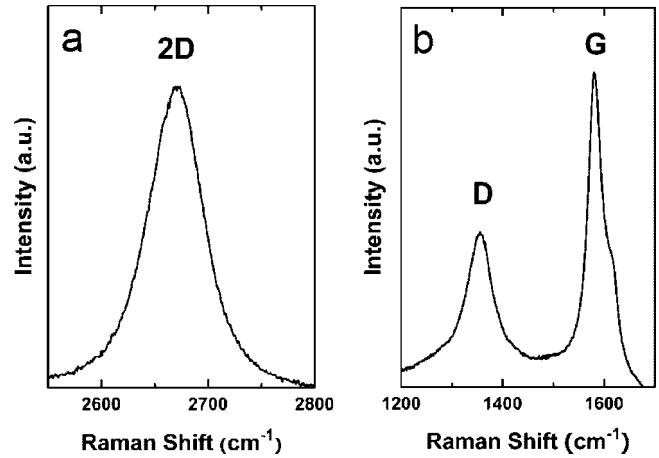

Figure 3. Raman spectroscopy characterization. Raman spectra of the synthesized graphene sheets in the region of the (a) 2D peak and (b) D and G peaks.

synthesized sheets (Figure 3b), the spectrum could not be used to accurately assess the degree of disorder in individual sheets. Edges of graphene sheets are always seen as defects, and peaks indicating a defective structure will appear in the spectra of perfect graphene sheets if the laser spot includes these edges.[29] The characterized samples consisted of multiple overlapping sheets (Figure 1c), and the presence of the additional peaks could have been the result of many edges captured by the 300 μm $\times$ 120 μm laser spot. Because of the overlapping nature of the graphene samples, an additional characterization method was needed to study individual sheets.

Individual graphene sheets were characterized using a recently developed method that combines scanning transmission electron microscopy (STEM) imaging with nanoarea parallel beam electron diffraction.[31] Diffraction patterns were

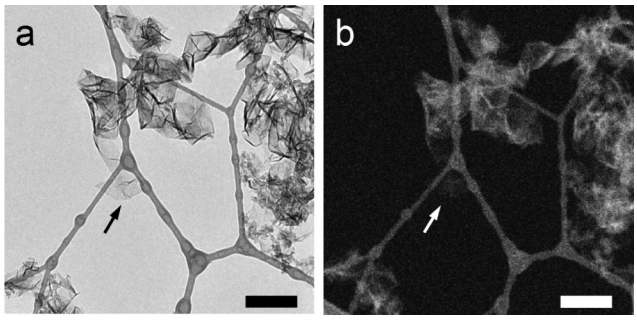

Figure 4. TEM and DF-STEM of overlapping graphene sheets. (a) TEM image of overlapping graphene sheets. (b) The corresponding high-angle dark-field STEM image of the overlapping sheets used as a map for electron diffraction characterization. The arrows indicate the region that was characterized by electron diffraction. Scale bars represent 100 nm.

obtained using a Zeiss Libra 200/FEG transmission electron microscope, operated at 200 kV with Koehler illumination. First, a region containing graphene sheets was located in TEM mode (Figure 4a). Next, using a condenser aperture of 15 μm and a convergent beam size of 5 nm, the high-angle dark-field STEM imaging function of the Libra was used to obtain a scanning image of the region (Figure 4b). To obtain a clear diffraction pattern, the STEM stationary beam function of the Libra was then utilized to form a small, nearly parallel beam with a diameter of 300 nm. The STEM image obtained in convergent beam mode (Figure 4b) was then used as a map to exactly position the parallel beam probe on any area of interest within the STEM image. This technique enabled us to obtain diffraction patterns of graphene sheets within the region. Diffraction patterns were recorded on a charge-coupled device (CCD).

The region indicated by an arrow in the TEM image (Figure 4a) and the corresponding STEM image (Figure 4b) consisted of folded and overlapping graphene sheets. A single diffraction pattern obtained from this region (Figure 5a) exhibited several sets of diffraction spots from several overlapping sheets that were locally normal to the incident beam. By use of the Miller−Bravais indices (*hkil*) for graphite, each set of diffraction spots exhibited an inner hexagon corresponding to indices (1−110) (2.13 Å spacing) and an outer hexagon corresponding to indices (1−210) (1.23 Å spacing).

A recent electron diffraction study of graphene[6] demonstrated that the intensity profiles of graphene diffraction patterns could be used to determine the number of layers in a graphene sheet. The relative intensities of diffraction spots in the inner and outer hexagons were shown to be equivalent in single-layer graphene.[6] The relative intensities of the spots in the outer hexagon were shown to be twice those of the spots in the inner hexagon for bilayer graphene.[6] A set of diffraction spots obtained from a synthesized graphene sheet is indicated by circles in Figure 5a. An intensity profile of equivalent Bragg reflections taken along the line denoted by

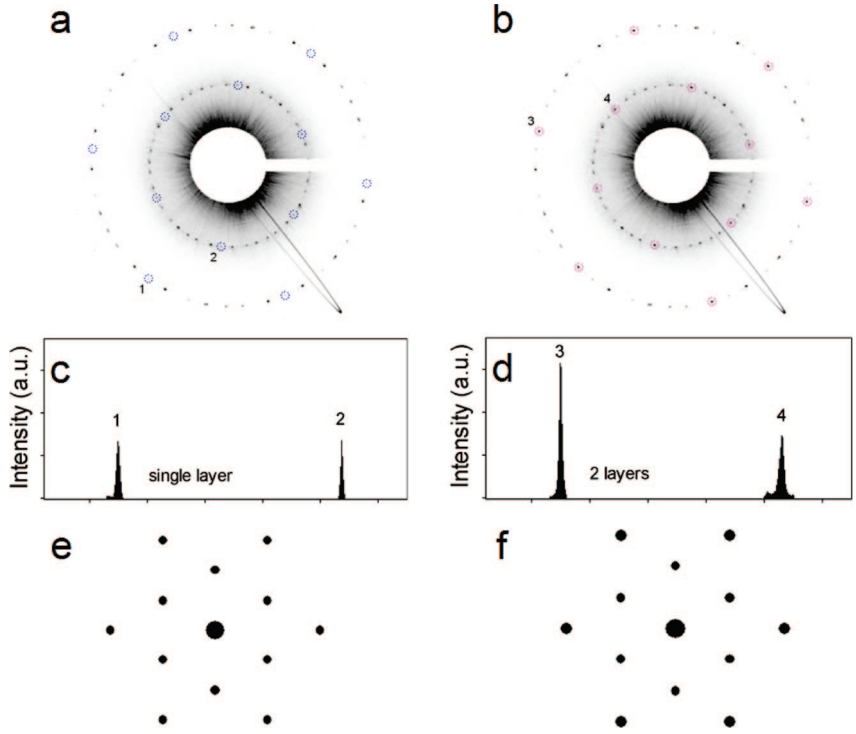

Figure 5. Electron diffraction characterization. (a) Diffraction pattern from a region containing several overlapping single-layer and bilayer graphene sheets. The single-layer graphene diffraction pattern is indicated by circles. (b) The same diffraction pattern with a bilayer graphene diffraction pattern indicated by circles. (c) Intensity profile of the diffraction spots along a line connecting points 1 and 2 in the single-layer graphene diffraction pattern. The uniform intensity profile between the inner and outer spots proves that the graphene sheet consists of a single layer. (d) Intensity profile of the diffraction spots along a line connecting points 3 and 4 in the bilayer graphene diffraction pattern. The spot in the outer hexagon is twice the intensity of the inner hexagon, indicating that the sheet is bilayer graphene. MacTempas simulation of diffraction patterns for (e) single-layer graphene and (f) bilayer graphene.

numbers 1 and 2 showed that the intensities of the inner and outer spots were equivalent (Figure 5c), indicating that the set of diffraction spots originated from a single-layer graphene sheet. Another set of diffraction spots present on the same diffraction pattern is circled in Figure 5b. An intensity profile taken along the line denoted by the numbers 3 and 4 (Figure 5d) showed that the intensity of the spot in the outer hexagon was twice the intensity of the spot in the inner hexagon, indicating that the set of diffraction spots corresponded to a bilayer graphene sheet.

To confirm our electron diffraction results, MacTempas software was used to obtain simulated diffraction patterns for single-layer (Figure 5e) and bilayer (Figure 5f) graphene. The simulated patterns agreed with the diffraction patterns obtained from the synthesized single-layer and bilayer sheets.

The combined results of the Raman measurements and electron diffraction patterns indicate that the quality of the synthesized graphene sheets was better than, or comparable to, graphene obtained by other methods. For instance, the intensity ratio of the D and G peaks in the Raman spectra of graphene has been shown to increase with the degree of disorder in the sheets.[29] Away from the edges, a perfect graphene sheet does not exhibit the D peak.[6] Our Raman measurements could not avoid the sample edges, and even then the peak ratio was 0.45 (Figure 3b), which is lower than the intensity ratios obtained from chemically reduced graphite oxide[8,9] and PECVD.[16,19,20] The latter materials had higher D peak intensities and intensity ratios that approached or exceeded unity. Furthermore, sheets obtained by PECVD methods possessed defective graphite structures[16,17] and nanographite domains,[18] and diffraction patterns obtained from these materials exhibited blurred diffraction spots, as well as rings originating from amorphous regions on the sheets. The synthesized single-layer and bilayer graphene sheets exhibited sharp, clear diffraction spots (Figure 5) that resembled diffraction patterns obtained from graphene sheets created by micromechanical cleavage.[6]

Previous studies[1–14] have proven that it is possible to create 2D graphene, and here it has been shown that single-layer and bilayer graphene sheets can be synthesized in the gas phase in a substrate-free environment. The atmospheric-pressure reactor used in our experiments is simple in operation and capable of continuously producing graphene. Numerous novel materials can be commercially produced[32,33] in atmospheric-pressure microwave plasma reactors, and here we have demonstrated the feasibility of producing atomically thin graphene sheets.

Acknowledgment. The research at the University of California was supported by the National Aeronautics and Space Administration. A.D., V.R., Z.L., and M.F. acknowledge support of the National Center for Electron Microscopy, Lawrence Berkeley Laboratory, which is supported by the U.S. Department of Energy under Contract # DE-AC02-05CH11231.

References

(1) Novoselov, K. S.; Geim, A. K.; Morozov, S. V.; Jiang, D.; Zhang, Y.; Dubonos, S. V.; Grigorieva, I. V.; Firsov, A. A. *Science* **2004**, *306*, 666.
(2) Novoselov, K. S.; Jiang, D.; Schiedin, F.; Booth, T. J.; Khotevich, V. V.; Morozov, S. V.; Geim, A. K. *Proc. Natl. Acad. Sci. U.S.A.* **2005**, *102*, 10451.
(3) Novoselov, K. S.; Geim, A. K.; Morozov, S. V.; Jiang, D.; Katsnelson, M. I.; Grigorieva, I. V.; Dubonos, S. V.; Firsov, A. A. *Nature* **2005**, *438*, 197.
(4) Novoselov, K. S.; McCann, E.; Morozov, S. V.; Fal'ko, V. I.; Katsnelson, M. I.; Zeitler, U.; Jiang, D.; Schedin, F.; Geim, A. K. *Nat. Phys.* **2006**, *2*, 177.
(5) Meyer, J. C.; Geim, A. K.; Katsnelson, M. I.; Novoselov, K. S.; Booth, T. J.; Roth, S. *Nature* **2007**, *446*, 60.
(6) Ferrari, A. C.; Meyer, J. C.; Scardaci, V.; Casiraghi, C.; Lazzeri, M.; Mauri, F.; Piscanec, S.; Jiang, D.; Novoselov, K. S.; Roth, S.; Geim, A. K. *Phys. Rev. Lett.* **2006**, *97*, 187401.
(7) Stankovich, S.; Dikin, D. A.; Dommett, G. H. B.; Kohlhaas, K. M.; Zimney, E. J.; Stach, E. A.; Piner, R. D.; Nguyen, S. T.; Ruoff, R. S. *Nature* **2006**, *442*, 282.
(8) Stankovich, S.; Dikin, D. A.; Piner, R. D.; Kohlhaas, K. A.; Kleinhammes, A.; Yuanyuan, J.; Wu, Y.; Nguyen, S. T.; Ruoff, R. S. *Carbon* **2007**, *45*, 1558.
(9) Kudin, K. N.; Ozbas, B.; Schniepp, H. C.; Prud'homme, R. K.; Aksay, I. A.; Car, R. *Nano Lett.* **2008**, *8*, 36.
(10) Berger, C.; Song, Z.; Li, X.; Wu, X.; Brown, N.; Naud, C.; Mayou, D.; Li, T.; Hass, J.; Marchenkov, A. N.; Conrad, A. H.; First, P. N.; de Heer, W. A. *Science* **2006**, *312*, 1191.
(11) Hass, J.; Feng, R.; Li, T.; Li, X.; Zong, Z.; de Heer, W. A.; First, P. N.; Conrad, E. H.; Jeffrey, C. A.; Berger, C. *Appl. Phys. Lett.* **2006**, *89*, 143106.
(12) Coraux, J.; N'Diaye, A. T.; Busse, C.; Michely, T. *Nano Lett.* **2008**, *8*, 565.
(13) Marchini, S.; Günther, S.; Wintterlin, J. *Phys. Rev. B* **2007**, *76*, 075429.
(14) Ueta, H.; Saida, M.; Nakai, C.; Yamada, Y.; Sasaki, M.; Yamamoto, S. *Surf. Sci.* **2004**, *560*, 183.
(15) Zhao, X.; Outlaw, R. A.; Wang, J. J.; Zhu, M. Y.; Smith, D.; Holloway, B. C. *J. Chem. Phys.* **2006**, *124*, 194704.
(16) Wang, J. J.; Zhu, M. Y.; Outlaw, R. A.; Zhao, X.; Manos, D. M.; Holloway, B. C. *Appl. Phys. Lett.* **2004**, *85*, 1265.
(17) Wang, J. J.; Zhu, M. Y.; Outlaw, R. A.; Zhao, X.; Manos, D. M.; Holloway, B. C. *Carbon* **2004**, *42*, 2867.
(18) Kobayashi, K.; Tanimura, M.; Nakai, H.; Yoshimura, A.; Yoshimura, H.; Kojima, K.; Tachibana, M. *J. Appl. Phys.* **2007**, *101*, 094306.
(19) Chuang, A. T. H.; Boskovic, B. O.; Robertson, J. *Diamond Relat. Mater.* **2006**, *15*, 1103.
(20) Chuang, A. T. H.; Robertson, J.; Boskovic, B. O.; Koziol, K. K. K. *Appl. Phys. Lett.* **2007**, *90*, 123107.
(21) Frenklach, M.; Kermatick, R.; Huang, D.; Howard, W.; Spear, K. E.; Phelps, A. W.; Koba, R. *J. Appl. Phys.* **1989**, *66*, 395.
(22) Weigle, J. C.; Luhrs, C. C.; Chen, C. K.; Perry, W. L.; Mang, J. T.; Lopez, G. P.; Phillips, J. *J. Phys. Chem. B* **2004**, *108*, 18601.
(23) Gleiman, S.; Chen, C. K.; Datye, A.; Phillips, J. *J. Mater. Sci.* **2002**, *37*, 3429.
(24) Berger, S. D.; McKenzie, D. R.; Martin, P. J. *Philos. Mag. Lett.* **1988**, *57*, 285.
(25) Duarte-Moller, A.; Espinosa-Magana, F.; Martinez-Sanchez, R.; Avalos-Borja, M.; Hirata, G. A.; Cota-Araiza, L. *J. Electron Spectrosc. Relat. Phenom.* **1999**, *104*, 61.
(26) Chu, P. K.; Li, L. *Mater. Chem. Phys.* **2006**, *96*, 253.
(27) Wirth, R. *Phys. Chem. Minerals* **1997**, *24*, 561.
(28) Gloter, A.; Zbinden, M.; Guyot, F.; Gaill, F.; Colliex, C. *Earth Planet. Sci. Lett.* **2004**, *222*, 947.
(29) Ferrari, A. C. *Solid State Commun.* **2007**, *143*, 47.
(30) Casiraghi, C.; Pisana, S.; Novoselov, K. S.; Geim, A. K.; Ferrari, A. C. *Appl. Phys. Lett.* **2007**, *91*, 233108.
(31) Haifeng, H.; Nelson, C. *Ultramicroscopy* **2007**, *107*, 340.
(32) Phillips, J.; Chen, C. K.; Kroenke, W. U.S. Patent 6,689,192, 2004.
(33) Phillips, J.; Perry, W. L.; Chen, C. K. U.S. Patent 6,998,103, 2006.

NL8011566